NASA TECHNICAL MEMORANDUM

NASA TM X-53391

February 7, 196

NASA TM X-53391

NEWTONIAN AERODYNAMICS FOR GENERAL BODY SHAPES WITH SEVERAL APPLICATIONS

By W.H. Heybey
Aero-Astrodynamics Laboratory

NASA

George C. Marshall Space Flight Center, Huntsville, Alabama

TECHNICAL MEMORANDUM X-53391

NEWTONIAN AERODYNAMICS FOR GENERAL BODY SHAPES WITH SEVERAL APPLICATIONS

By

W. H. Heybey

George C. Marshall Space Flight Center

Huntsville, Alabama

ABSTRACT

The Aero-Astrodynamics Research Review No. 2 (NASA TM X-53295) contains a succinct account of Newtonian aerodynamics for general analytical surfaces. Much of the detail passed over there when dealing with applications, together with a more thorough exposition of the general approach, is given in the present report which, it is hoped, will be useful to those who wish to actually work with Newtonian's method. It ought to serve well in the high-Mach number, low-density phase of re-entry flight. The lemniscatic body chosen in the Research Review paper as an example for calculating blunt-nose forces is replaced here by a circular cone with spherical base cap, since this configuration seems to command more immediate interest.

NASA - GEORGE C. MARSHALL SPACE FLIGHT CENTER

NASA - GEORGE C. MARSHALL SPACE FLIGHT CENTER

Technical Memorandum X-53391

February 7, 1966

NEWTONIAN AERODYNAMICS FOR GENERAL BODY SHAPES WITH SEVERAL APPLICATIONS

By

W. H. Heybey

TECHNICAL AND SCIENTIFIC STAFF
AERO-ASTRODYNAMICS LABORATORY

TABLE OF CONTENTS

LIST OF SYMBOLS (Partial)

A. General: Vector quantities are denoted by underlining, except the unit vectors

$$\mathbf{i},\ \mathbf{j},\ \mathbf{k}$$

on the axes of a Cartesian rectangular system.

α: overall angle of attack

α_{loc}: angle of attack at an elemental surface

α': its complement

$\underline{n}$: unit vector in direction of the surface interior normal (components, n_1, n_2, n_3)

$\underline{\nu}$: unit vector in flow direction (components α_1, α_2, α_3)

ρ_∞, V_∞, q_∞: density, velocity, dynamic pressure in undisturbed flow

C_p: local pressure coefficient

σ, τ: coordinates in a surface system

dS: elemental surface

$d^2\underline{P}$: elemental force acting on dS

$\underline{P}$: total force (components X, Y, Z)

O: origin and point of reference for force moments

$\underline{r}$: radius vector from O to dS

$\underline{M}$: moment integral of elemental forces

$\underline{M}^*$: moment of total force

$\underline{r}^*$: its arm

s_t: tangential shadow curve

s_c: cast shadow curve

B. Elliptical Cone: Origin at tip; flow toward it.

a: length unit on x-axis (which is taken as cone axis)

σ: surface coordinate, here also serving as multiplicator to express abscissas x in terms of a

b, c: elliptical semi-axes at $\sigma = 1$; $b > c$

B, C: semi-axes of cone base (where $\sigma = \sigma_b$)

ϵ: numerical excentricity of the elliptical cross sections

ω: angle made by top meridian and cone axis (tip angle)

$q = \epsilon^2 \cos^2\omega$

x^*: abscissa of centroid if placed on cone axis.

C. Coaxial Cylindrical Afterbody: Origin at cone tip (as above).

$\tilde{B}$, $\tilde{C}$: semi-axes of its cross section, parallel to B and C; $\tilde{B}$, $\tilde{C} \leqq B$, C

$\lambda = (\tilde{C}/B)^2$

σ, $\tilde{\tau}$: surface coordinates on cylinder

$x_b = a\sigma_b$: cone length

$x_c = a\sigma_c$: total length of composite body

$h = a(\sigma_c - \sigma_b)$: cylinder length

$\sigma = \psi(\tilde{\tau})$: equation of cast shadow curve on cylinder

$\tilde{\tau} = 0$: tangential shadow line on cylinder

R: cross sectional radius if cylinder is circular; $R \leqq C$

$\beta = R/B$

$\underset{\sim}{\tilde{Z}}$: force acting on cylinder

$\underset{\sim}{\tilde{M}}$: its moment with respect to cone tip

$\tilde{x}^*$: abscissa of cylinder centroid

x^*_{tot}: centroid abscissa of composite body (cone and afterbody)

D. Biparabolic Conoid: Origin at tip; flow toward it.

a: parabola parameter, used as unit length

ω: angle made by top meridian and conoid axis (tip angle)

$\hat{B}$, $\hat{C}$: "semi-axes" of biparabolic base (Figure 4)

$x_b = 2a\sigma_b^2$: conoid length

χ: wedge angle made by the x,y-plane and any plane through y-axis

$$m = \sqrt{(x_b/a) \sin 2\omega}$$

$$A = \frac{(1 + m^2) \arctan m - m}{m^3}$$

$$K = \sqrt{1 + (x_b/B)^2}$$

B: see Elliptical Cone

x^*: abscissa of centroid if placed on conoid axis.

E. Circular Cone with Spherical Sections Capping Its Base: Origin at sphere nose; flow toward it.

B, R: cone base and sphere radii

a: cone length

x_b: distance of cone base from origin

μ, ρ: surface coordinates on sphere

σ, $\tilde{\rho}$: surface coordinates on cone

$\tilde{\rho}^*$: defines tangential shadow meridian on cone

X, $\tilde{Y}$: y-components of the total forces acting on spherical cap and cone, respectively

$\tilde{x}^*$: centroid abscissa of cone alone

x^*_{tot}: centroid abscissa of composite body (capped cone)

F. <u>The Modified Approach</u>: $\alpha \approx 0°$.

ω: local angle of attack at stagnation point

C_p^*: pressure coefficient at stagnation point

C_p: pressure coefficient elsewhere

M_∞: Mach number in undisturbed flow

γ: ratio of specific heats in the gas

σ_s: angle between attached shock and axis of a pointed body of revolution (shock angle)

$K = M_\infty \omega$

$K_s = M_\infty \sigma_s$

TECHNICAL MEMORANDUM X-53391

NEWTONIAN AERODYNAMICS FOR GENERAL BODY SHAPES WITH SEVERAL APPLICATIONS

SUMMARY

In the hypersonic regime the Newtonian flow model, especially in its modified form, has been known for some time to produce satisfactory results regarding a number of basic body shapes. It may reasonably be expected to also work well with more complicated body geometries as presented, e.g., by re-entry vehicles. Because of its simplicity, the components of the aerodynamic force and the location of the centroid can be calculated without the elaborate effort otherwise required in gas dynamics. The mathematics pertaining to the unmodified approach have been developed here for a general surface given in analytic terms. Applications have been worked out to the elliptic cone, first without, then with an attached rear cylinder, to a conoid of biparabolic cross sections, and to a blunt body resembling the Apollo capsule. The modification merely amounts to improving a constant; it has been described in the last section where a survey of results as compared with known data is also given.

I. INTRODUCTION

The Newtonian concept substitutes for the flowing liquid an assemblage (point mass array) of many minute inelastic particles all moving with equal and parallel velocities. On contact with a material object such particles transfer their momenta components normal to the surface while they retain their tangential momenta carrying them off without further effect unless there is a secondary impingement by the deflected stream. There is no action on the body except by direct hits; no pressure exists on surface elements shielded by upstream elements (contrary to later experimental evidence). The formation of a shock, which of course was unknown in Newton's time, is even now not contemplated in simple impact theory.

This theoretical picture of a flowing liquid and of its actions on body surfaces had soon to be abandoned in hydrodynamics. It is also inadequate with gas flows, both subsonic and supersonic. But in the hypersonic regime, the expressions derived from it for the surface pressure distribution and concomitant aerodynamic data yield values often surprisingly close to those observed experimentally or obtained by more exact theoretical means. In recent times Newton's method is freely used

in dealing with such flows; it offers closed-form results available in a relatively easy manner. It has been found wanting, however, with surfaces concave to flow direction and in gases with exceptionally low ratio of specific heats approaching unity (for explanation and examples, see Reference 1, p. 125-128). Applications seem best restricted therefore to bodies turning convex surface parts toward an onrushing gas of ordinary description. The simple theory can often be improved upon by introducing a correction to the local pressure coefficient based on shock transition relations (modified method). A dependence on Mach number, absent so far, then appears.

A hypersonic regime should prevail for some time when a space vehicle, approaching the earth with quasi-cosmic velocity, moves in the uppermost regions of the continuum atmosphere. One would like to predict theoretically the lift and drag the body will experience in these regions, together with the stability behavior as depending on the location of the center of pressure.

However, the body shapes considered in the literature are mostly of the simple kind, such as circular cones and cylinders, spheres, diamond-shaped wing profiles, blunted cones and capped cylinders. There appears to be a need to systematize the method for application to more complex structures. In the following, the Newtonian expressions will be derived for an unspecified general surface which is allowed to be composite. The stipulation is made that all its parts can be described by analytic equations. Surface zones hit by secondary incidence are not permitted to exist. Applications will be made to the elliptical cone (with and without cylindrical appendage), to a conoid of biparabolic cross sections, and to a blunt-nosed body of the Apollo capsule types.

II. IMPACT FLOW MATHEMATICS IN GENERAL

The angle of attack, α, is commonly understood as the angle made by the direction of the uniform flow with a line chosen within the body, usually the body's axis if such an axis can be defined. In conventional aerodynamics there is rarely occasion to consider other angles relative to flow direction, since it affects the pressure distribution only indirectly by way of boundary conditions. But in impact flow where every elemental surface, if hit at all, is hit from a well-defined direction bearing on the elemented force transferred, a local angle of attack must be defined which will depend on the position of the local surface element as indicated by its interior normal. Let the latter's direction be given by the unit vector

$$\underline{n} = n_1 i + n_2 j + n_3 k \qquad (1)$$

where i, j and k are unit vectors on the axes of the Cartesian system in which the body's surface is described. The unit vector, $\underline{\nu}$, in flow direction will usually be linked to the position of the axis; its expression will then contain certain trigonometric functions of α which cannot be obtained before a particular body-flow configuration is considered. At this station we therefore write, in general,

$$\underline{\nu} = \alpha_1 i + \alpha_2 j + \alpha_3 k. \tag{2}$$

The two vectors $\underline{n}$ and $\underline{\nu}$ define the local plane of incidence which is normal to the elemental surface and intersects with its tangential plane in a straight line, t. The angle t makes with the direction $\underline{\nu}$ is, in general, considered the local angle of attack, α_{loc}. More convenient to handle, however, is its complement

$$\alpha' = \frac{\pi}{2} - \alpha_{loc} \tag{3}$$

since α', as the acute angle between flow direction and the interior normal*, is easily obtainable from the scalar product

$$\cos \alpha' = \underline{n} \cdot \underline{\nu} = \sum_{i=1}^{3} n_i \alpha_i. \tag{4}$$

In this way one eliminates the somewhat bothersome task of determining the line t which, except for α_{loc}, has little interest, whereas $\underline{n}$ gives the direction of the local force. To be sure, the tangential momentum of the striking particle is carried away in the direction of t, but that momentum component is ineffective, secondary hits not being admitted.

Aside from terms small of second order, the local pressure coefficient will be that of a flat plate under the angle of attack α_{loc}. Newton's second law, if applied to normal momentum transfer, gives the expression

$$C_p = 2 \sin^2 \alpha_{loc} \tag{5}$$

*The interior normal, if defined as the axis of the elemental surface, would give α' the meaning of local angle of attack in agreement with the definition of the overall angles.

which, through relations (3) and (4) goes into

$$C_p = 2(\underline{\nu} \cdot \underline{n})^2. \tag{6}$$

Expression (5) is well known (Reference 2, p. 6); it uses the continuum notion of density to describe the mass of the particles per unit volume of the incoming flow. The elemental force, as usual, is obtained from the coefficient C_p by multiplying it with the local surface element, dS, and with the dynamic pressure,

$$q_\infty = \frac{\rho_\infty V_\infty^2}{2}, \tag{7}$$

of the undisturbed flow which is taken as known. Thus,

$$d^2\underline{P} = 2q_\infty(\underline{\nu} \cdot \underline{n})^2 \, dS \, \underline{n}. \tag{8}$$

The local force is small of second order and points into the direction $\underline{n}$. The determination of $\underline{n}$ and dS calls for the methods developed in the differential geometry of surfaces. Here, lucid and symmetric formulations emerge when the surface is given a point-wise representation

$$\left.\begin{aligned} x &= x(\sigma,\tau) \\ y &= y(\sigma,\tau) \\ z &= z(\sigma,\tau) \end{aligned}\right\}. \tag{9}$$

The variables σ and τ will move within certain "natural" intervals in order for the Cartesian triplets x, y, z to exactly embrace the surface points. Often, σ and τ will be found by geometric reasoning which may lead to a clearer visualization of surface features and, by the way, may suggest several attractive ways of introducing these variables. On the other hand, one might be quite formal about it, putting $x = \sigma$, $y = \tau$, $z = f(\sigma,\tau)$.

Representation (9) offers the additional advantage that, on assigning parametric values to τ or to σ, it defines two sets of parametric curves on the surface

$$\left.\begin{aligned} x_1 &= x(\sigma,\tau^*), \quad & y_1 &= y(\sigma,\tau^*), \quad & z_1 &= z(\sigma,\tau^*) \\ x_2 &= x(\sigma^*,\tau), \quad & y_2 &= y(\sigma^*,\tau), \quad & z_2 &= z(\sigma^*,\tau) \end{aligned}\right\} \tag{10}$$

which constitute a curvilinear (not necessarily orthogonal) system of coordinates on it. The lines (10) are individualized by the choice of τ^* and σ^* at which point they intersect. In general, they must be expected to be of double curvature (spatial curves). However, they can often be taken as meridians and cross-sectional peripheries, in which case both sets are planar. If in doubt one may consult the determinant

$$\begin{vmatrix} x' & y' & z' \\ x'' & y'' & z'' \\ x''' & y''' & z''' \end{vmatrix} = \Delta \tag{11}$$

where the primes denote differentiation with respect to the one quantity, σ or τ, which is variable in the set considered. If $\Delta = 0$, that set consists of plane curves. It is seen that if, e.g., the surface representation (9) depends in the second degree at most on σ, the curves $\tau^* = \text{const.}$ will be planar. One can then use one of the planes for a two-dimensional representation of the curve it contains and thus make the latter's shape and course on the surface more clearly understood.

The surface functions (9) depend on both the variables σ and τ. Partial derivatives with respect to them will be indicated by corresponding subscripts.

Regarding first the vector $\underline{n}$, its components follow from the set (9) as

$$\left.\begin{aligned} n_1 &= \frac{1}{\pm N}\begin{vmatrix} y_\sigma & z_\sigma \\ y_\tau & z_\tau \end{vmatrix}, \quad n_2 = \frac{1}{\pm N}\begin{vmatrix} z_\sigma & x_\sigma \\ z_\tau & x_\tau \end{vmatrix}, \quad n_3 = \frac{1}{\pm N}\begin{vmatrix} z_\sigma & y_\sigma \\ x_\tau & z_\tau \end{vmatrix} \\ \text{where} \quad N &= \left| \sqrt{\begin{vmatrix} y_\sigma & z_\sigma \\ y_\tau & z_\tau \end{vmatrix}^2 + \begin{vmatrix} z_\sigma & x_\sigma \\ z_\tau & x_\tau \end{vmatrix}^2 + \begin{vmatrix} x_\sigma & y_\sigma \\ x_\tau & y_\tau \end{vmatrix}^2} \right| . \end{aligned}\right\} \tag{12}$$

The sign appropriate to the interior normal can be fixed without difficulty once the functions (9) are known for a particular surface.

Secondly, the elemental surface is given by

$$dS = N\, d\sigma\, d\tau \tag{13}$$

where $d\sigma$, $d\tau$ should be introduced as positive increments (the later integrations must be performed over intervals in which σ and τ increase).

The second order force differential (9) may now be written as

$$\begin{aligned} d^2\underline{P} &= 2q_\infty(n_1\alpha_1 + n_2\alpha_2 + n_3\alpha_3)^2\, N(in_1 + jn_2 + kn_3) \\ &\equiv i\, d^2X + j\, d^2Y + k\, d^2Z \end{aligned} \tag{14}$$

where the components X, Y, Z of the total force $\underline{P}$ are often called the "chordwise," "lateral," "normal" forces, respectively. These terms imply that the chord is taken as the x-axis and that $\underline{\nu}$ has no component in y-direction (rather than z-direction). They must be exchanged with different correlations, and may even lose meaning altogether with highly irregular bodies. But in any case the determination of $\underline{P}$ is reduced to a double quadrature which can always be carried out either analytically, or, failing that, numerically.

In addition to the resulting force $\underline{P}$ there will be a resulting moment of the elemental forces:

$$\underline{M} = \int\int [\underline{r} \times d^2\underline{P}] \tag{15}$$

where

$$\underline{r} = ix(\sigma,\tau) + jy(\sigma,\tau) + kz(\sigma,\tau)$$

is the lever arm from the origin (serving as the reference point) to the elemental surface, $dS(\sigma,\tau)$ where $d^2\underline{P}$ is attacking.

From the condition that $\underline{M}$ should be equal to the moment of the resulting force,

$$\underline{M}^* = [\underline{r}^* \times \underline{P}], \tag{16}$$

the arm

$$\underline{r}^* = ix^* + jy^* + kz^*$$

of the resulting force can be calculated. However, there are infinitely many of such arms, since a force may be moved along its line of attack without changing either the translatory or the rotatory effect. Mathematically, one of the $\underline{r}^*$-components remains indeterminate. An additional condition

$$f(x^*, y^*, z^*) = 0 \tag{17}$$

may be arbitrarily set up which in symmetrical configurations usually follows from the desire to have the point of $\underline{r}^*$ (the centroid) on the body axis.

Integration Limits

While the foregoing formulas are perfectly general and directly applicable to any analytic surface (or surface part), the determination and proper treatment of shielded areas often require painstaking detail work, especially if there are several such areas (which may or may not overlap). The problem remains simple when the "shadow" is a single point or an open line (enclosed area zero), because then the reduction in force is a zero quantity, and the natural σ- and τ-intervals can still be used when integrating.

Two types of shielded zones can be distinguished: those created by the bulk of the body as it opposes itself to the stream (tangential shadow curve), and those caused by the shadow cylinders through this curve and through sharp rims or edges that may exist on the surface (cast shadow).

With the first type, the grazing flow vector will reside in a plane tangential to the surface and thus be perpendicular to the interior normal at the point of contact. It then has to satisfy the condition

$$\underline{v} \cdot \underline{n} = 0. \tag{18}$$

This relationship of σ and τ, if written as $\tau = \varphi(\sigma)$ and introduced into the function (9), defines the points of the tangential shadow curve, s_t, in terms of σ.

The natural limits of the σ- and τ-intervals, if traced in a (σ,τ)-diagram, delineate a usually rectangular image of the surface. The curve $\tau = \varphi(\sigma)$ cuts off impact-free portions from this rectangle which must be excluded in integrating the force and moment differentials and thus changes the integration limits. Sometimes equation (18) will have the simple solutions σ = const. and/or τ = const., so that the integration area remains a narrowed-down rectangle. In the more complex cases involving a curved shadow boundary the integration will often have to be carried out numerically.

The root line of a shadow cylinder, as any spatial curve, can be described through the variation of a single variable, ξ:

$$x_c = f_1(\xi),\ y_c = f_2(\xi),\ z_c = f_3(\xi).$$

Care should be taken to determine the interval in which ξ may move in order to account for that length of the line that is exposed to the particle stream. If the curve is part of the surface (9), as with the rim of truncated bodies, the variable ξ can be identified with either σ or τ (fin edges, e.g., would not usually permit this).

The straight lines

$$\frac{x - x_c}{\alpha_1} = \frac{y - y_c}{\alpha_2} = \frac{z - z_c}{\alpha_3} \tag{19}$$

in flow direction define the curved surface of the shadow cylinder; their intersections with other portions of the body surface, if they exist, form an additional shadow boundary, s_c, which, in handling the integration limits, must be considered together with any shadow boundary, s_t, consequent to tangential incidence and determined by equation (18). An example of this is found in Section IV.

III. THE ELLIPTICAL CONE IN SIMPLE IMPACT FLOW

With the tip of the cone at the origin and its axis coinciding with the x-axis (Figure 1), its equation can be written as

$$\frac{y^2}{b^2} + \frac{z^2}{c^2} = \frac{x^2}{a^2} \tag{20}$$

implying that the cross section at any station x = const. is always an ellipse with axis ratio b/c. The lengths of the half axes at the base are denoted by B and C. Surface points with $x < 0$ will not be considered.

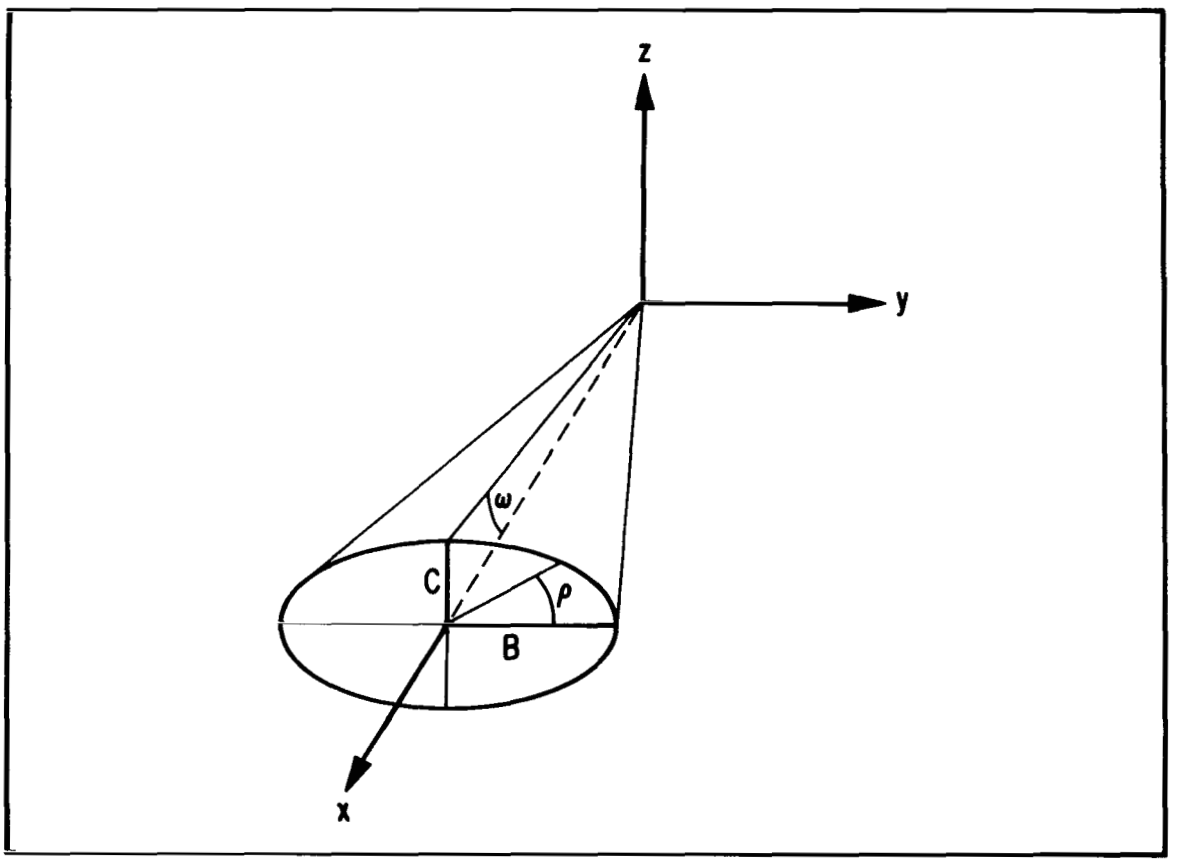

Figure 1. The Elliptical Cone

One verifies easily that the coordinate triplets connected by equations (20) can be represented as

$$\left.\begin{aligned} x &= a\sigma \\ y &= b\sigma \cos \tau \\ z &= c\sigma \sin \tau \end{aligned}\right\}. \tag{21}$$

The variable σ here is a pure number that counts the distance x from the origin in terms of the unit a. If $\sigma = \sigma_b$ identifies the distance of the base ($x_b = a\sigma_b$ being the cone length), the variable σ will range in

$$0 \leqq \sigma \leqq \sigma_b$$

which is its natural interval. The parametric lines $\sigma = \sigma^*$ (second family is the set (10)) are cut out by planes parallel to the (y,z)-plane; they are the cross sectional ellipses of the cone. Condition (11) for planar curves is satisfied, since the differential quotients of x with respect to τ are all zero.

The surface lines $\tau = \tau^*$ (first family) are also planar (x, y, z depend linearly on σ). They pass through the origin, since σ can become zero. Their planes

$$cy \sin \tau^* = bz \cos \tau^*, \tag{22a}$$

being parallel to the x-axis, therefore intersect on it. Any one of these meridional planes defines two generating lines, members of the first family. If it makes the angle, ρ, with the (x, y)-plane (Figure 1), it can also be described by the equation

$$z = y \tan \rho. \tag{22b}$$

It follows that

$$b \tan \rho = c \tan \tau \tag{23}$$

where τ has been written for τ^*, since τ^* can be any of the angles τ.

To clarify the meaning of τ geometrically, consider Figure 2, which uses the cross sectional area at the distance $\sigma = 1$. The plane (22b) intersects with the elliptical circumference at point R. The point $\tilde{R}$ is on a circle of radius b concentric with the ellipse and has the y-coordinate in common with R($\tilde{y} = y$). To show that the angle τ, as indicated in Figure 2, bears the relationship (23) with ρ we note that the condition $\tilde{y} = y$, if introduced into the equations of the circle and the ellipse, requires that

$$\tilde{z} : b = z : c.$$

But $\tilde{z} = b \sin \tau$, so that $z = c \sin \tau$. Furthermore, $\tilde{y} = y = b \cos \tau$.

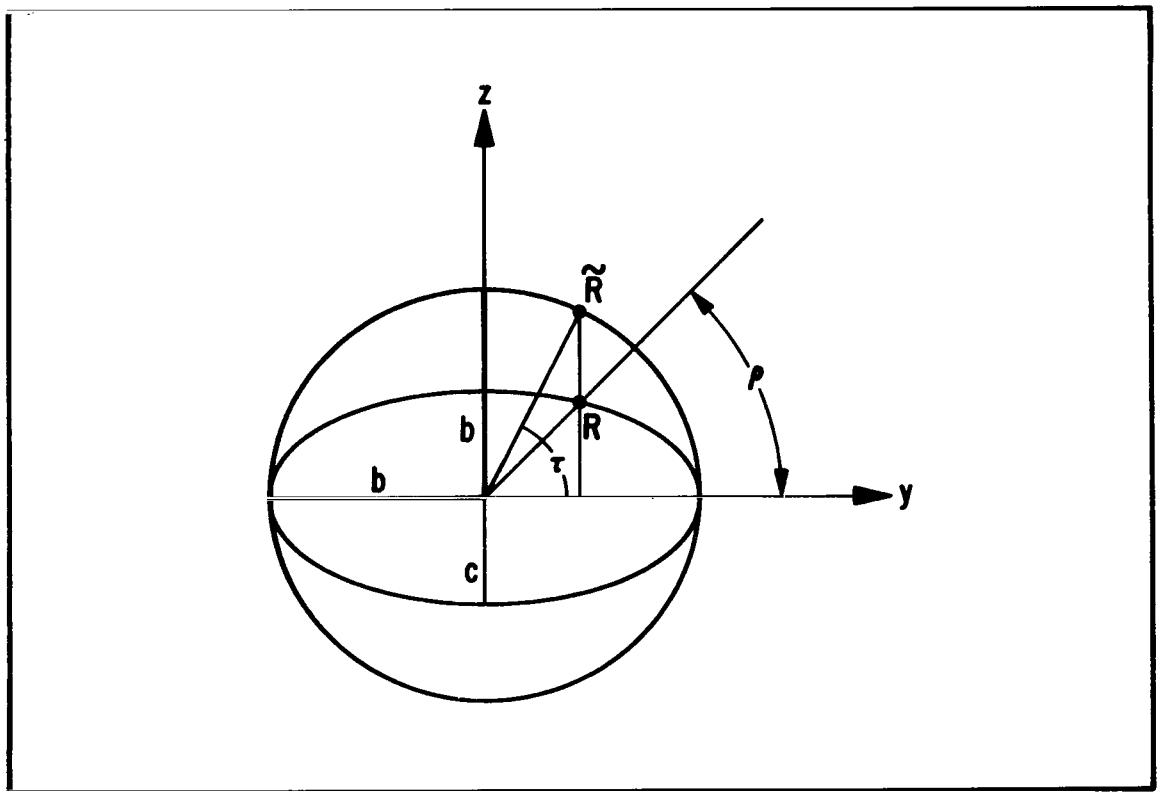

Figure 2. Relationship of τ and ρ

Finally,

$$\frac{z}{y} = \tan \rho = \frac{c}{b} \tan \tau,$$

which is the relation (23).

The meaning of the angle τ now being seen, its range when R moves round the full elliptical circumference may be given as

$$-\pi \leqq \tau \leqq \pi. \tag{24a}$$

If for simplicity we assume that the flow is parallel to the (z, x)-plane,

$$\underline{\nu} = i \cos \alpha + k \sin \alpha, \tag{25}$$

the incidence will be from below and behind as long as $0 \leqq \tau \leqq \pi/2$. The right half only of the cone needs to be considered in that case, provided that the chordwise and normal components are doubled (the lateral components cancel, $Y = 0$). The τ-interval is then narrowed down to

$$-\frac{\pi}{2} \leqq \tau \leqq \frac{\pi}{2}. \tag{24b}$$

The components of the interior normals are found from the general expressions (10) as applied to the surface (21):

$$\left.\begin{aligned} n_1 = \frac{bc\sigma}{N}, \quad n_2 = -\frac{ac\sigma \cos \tau}{N}, \quad n_3 = -\frac{ab\sigma \sin \tau}{N} \\ N = +\sigma \sqrt{b^2c^2 + c^2a^2 \cos^2\tau + a^2b^2 \sin^2\tau} \end{aligned}\right\}. \tag{26}$$

The signs have been chosen such that the x-component is always positive, as it evidently must be (Figure 1).

The shadow of the cone's base rim does not strike the surface and may be disregarded. But a tangential shadow boundary may exist. Condition (18) can be put into the form

$$\sin \tau_t = \frac{c}{a} \operatorname{cotg} \alpha. \tag{27}$$

Since the right side is constant, the shadow line will coincide with the generatrix $\tau = \tau_t$. Now by Figure 1,

$$\tan \omega = \frac{z}{x}\bigg|_{\tau = \frac{\pi}{2}} = \frac{c}{a} .$$

Consequently, there is no real solution for τ_t if $\alpha < \omega$; no shadow develops, and the cone is impinged on in its entirety. The τ-integration will have to extend over the natural interval (24b). However, when $\alpha > \omega$, this region shrinks to

$$-\frac{\pi}{2} \leqq \tau \leqq \tau_t$$

with $\tau_t \to \pi/2$ if $\alpha \to \omega$. The part of the upper surface half lying between the generatrices $\tau = \tau_t$ and $\tau = \pi/2$ is then shielded from the flow; it grows larger with increasing values of α and comprises the entire top of the right half-cone if $\alpha = 90°$ ($\tau_t = 0$).

The σ-interval is evidently not affected by the presence of the shadow line s_t.

In writing down the expressions for the two non-zero force components it is convenient to use the abbreviation

$$q = \epsilon^2 \cos^2 \omega$$

where

$$\epsilon = \sqrt{\frac{b^2 - c^2}{b^2}} \quad (b > c)$$

is the common numerical eccentricity of the ellipses. It then follows from the expressions (14), (25), (26) that

$$d^2X = -4q_\infty \, bc\sigma \, d\sigma \, \frac{(\sin\omega\cos\alpha - \cos\omega\sin\alpha\sin\tau)^2}{1 - q\cos^2\tau} \, d\tau$$

$$d^2Z = -4q_\infty \, ab\sigma \, d\sigma \, \frac{(\sin\omega\cos\alpha - \cos\omega\sin\alpha\sin\tau)^2}{1 - q\cos^2\tau} \sin\tau \, d\tau.$$

On integrating over the intervals $0 \leqq \sigma \leqq \sigma_b$ and $-\pi/2 \leqq \tau \leqq \tau_t$, the force coefficients, if referred to the base area

$$\pi \, bc \, \sigma_b^2 = \pi BC,$$

are found as

$$\left.\begin{aligned} C_X &= \frac{2}{\pi}\frac{\sin^2\alpha}{\epsilon^2}\left\{\frac{\pi}{2} + \tau_t + \sqrt{q}\,\operatorname{tg}\omega\operatorname{cotg}\alpha \ln\frac{1+\sqrt{q}\cos\tau_t}{1-\sqrt{q}\cos\tau_t} + \right. \\ &\left. + \frac{q}{\sqrt{1-q}}\left(\operatorname{tg}^2\omega\operatorname{cotg}^2\alpha - \frac{1-q}{q}\right)\left(\frac{\pi}{2} + \arctan\frac{\tan\tau_t}{\sqrt{1-q}}\right)\right\} \\ C_Z &= \frac{2}{\pi}\frac{\sin^2\alpha}{\epsilon^2\tan\omega}\left\{\cos\tau_t + \frac{\sqrt{q}}{2}\left(\operatorname{tg}^2\omega\operatorname{cotg}^2\alpha - \frac{1-q}{q}\right)\ln\frac{1+\sqrt{q}\cos\tau_t}{1-\sqrt{q}\cos\tau_t} + \right. \\ &\left. + 2\operatorname{tg}\omega\operatorname{cotg}\alpha\left[\frac{\pi}{2} + \tau_t - \sqrt{1-q}\left(\frac{\pi}{2} + \arctan\frac{\tan\tau_t}{\sqrt{1-q}}\right)\right]\right\}. \end{aligned}\right\} \quad (28)$$

The principal value (in $<-\frac{\pi}{2}, \frac{\pi}{2}>$) of the arc tan-function must be taken here. The numerical value of τ_t follows from relation (27). Expressions (28) need be used only with $\alpha > \omega$. They simplify considerably when there is no tangential shadow zone on the surface ($\alpha \leqq \omega$; $\tau_t = \pi/2$) and can then be set into the form

$$\left.\begin{aligned} C_X &= 2 \left\{ \frac{1 - \sqrt{1 - q}}{q} \sin^2\alpha \cos^2\omega + \frac{\cos^2\alpha \sin^2\omega}{\sqrt{1 - q}} \right\} \\ C_Z &= 2 \sin 2\alpha \cos^2\omega \frac{1 - \sqrt{1 - q}}{q} \end{aligned}\right\} \quad \alpha \leqq \omega. \qquad (29)$$

The known formulas for the circular cone (Reference 2, p. 80-84) are obtained from expressions (28) and (29) by letting q approach zero.

On account of the symmetrical configuration, the total force $\underline{P} = iX + kZ$ is in the (z,x)-plane and can be split there in two components, one in the direction of incidence (drag), the other perpendicular to it (lift), the coefficients becoming

$$\left.\begin{aligned} C_D &= C_X \cos\alpha + C_Z \sin\alpha \\ C_L &= -C_X \sin\alpha + C_Z \cos\alpha \end{aligned}\right\}. \qquad (30)$$

There is no lift with $\alpha = 0$.

By somewhat laborious integrations it can be shown that the moment (15), needed for the determination of the centroid, has neither an i- nor a k-component. From the symmetry of the flow-body configuration, one would indeed expect that the moment should seek to turn the body about an y-axis parallel. It attains the form

$$\underline{M} = \frac{4}{3} q_\infty \, j \, b(a^2 + c^2) \, \sigma_b^2 \, F(\tau_t)$$

where the integral

$$F = \int_{\tau=-\frac{\pi}{2}}^{\tau_t} \frac{(\sin\omega\cos\alpha - \cos\omega\sin\alpha\sin\tau)^2}{1 - q\cos^2\tau} \sin\tau\, d\tau$$

also appears in the Z-component of the total force which may be written as

$$Z = -2q_\infty ab\sigma_b^2 F(\tau_t).$$

The moment (16) of the total force emerges as

$$\underline{M}^* = \begin{vmatrix} i & j & k \\ x^* & y^* & z^* \\ X & 0 & Z \end{vmatrix} = y^*(iZ - kX) - j(x^*Z - z^*X).$$

Requiring $\underline{M}^* = \underline{M}$ one sees that y^* must be zero. This is understandable, since the force $\underline{P}$ is in the (z,x)-plane, its arm $\underline{r}^*$ (relative to 0) must have the same property. Moreover, if we let the force attack at a point of the body- (x-)-axis, the arm will be part of the latter

$$z^* = 0.$$

This is the form taken here by the condition (17). The equality of moments then leads to

$$x^* = \frac{|\underline{M}|}{-Z} = \frac{2}{3} a\sigma_b \left(1 + \frac{c^2}{a^2}\right) = \frac{2}{3} \frac{x_b}{\cos^2\omega}. \qquad (31)$$

The location of the centroid depends only on the length, x_b, of the cone and on the half-angle ω. With these parameters preserved, it does not vary if the angle of attack or the elliptical shape, or both, are changed. The formula is known for circular cones, but often derived employing the normal forces alone* and then does not contain the denominator $\cos^2\omega$, which indeed is negligible for small values of ω. Yet it will be noted that, with a 35-degree cone, the centroid is already close to the base and moves out of the body if ω is increased further. Since the mass center is at $\frac{3}{4}\, x_b$, slender cones are not stable. Stability begins at $\omega \approx 20$ degrees.

The restriction to the symmetric case maintained so far is tantamount in real flight to permitting pitch angles only. If it is desired to consider yawed and rolled positions as well, one may use the same body-fixed (x,y,z)-system as before. The unit vector, $\underline{\nu}$, of incidence, however, will have the general form (2) where the direction cosines α_i are determined by the instantaneous flight direction. The simple shadow boundary condition (27) will be replaced by

$$\sum n_i\, \alpha_i = 0,$$

and the discussion of integration limits will become less straightforward; both lower and upper boundaries of τ might be affected. The integrations can still be carried out analytically, as the force differential assumes the form

$$d^2\underline{P} = 2abcq_\infty \frac{\left(\frac{\alpha_1}{a} + \frac{\alpha_2}{b}\cos\tau - \frac{\alpha_3}{c}\sin\tau\right)^2}{\frac{1}{a^2} + \frac{\cos^2\tau}{b^2} + \frac{\sin^2\tau}{c^2}} \left(\frac{i}{a} - \frac{j\cos\tau}{b} - \frac{k\sin\tau}{c}\right) d\tau\, \sigma d\sigma.$$

Closed expressions for the force components can be obtained from a table of indeterminate integrals. The Y-component is no longer identically zero, and the full range (24a) for τ must be retained when seeking out the integration limits.

*See Ref. 2, p. 84. Mr. E. Linsley seems to have been among the first to insist that the chordwise forces can make a significant contribution to the moment $\underline{M}$ of a circular cone.

IV. CYLINDRICAL AFTERBODY ATTACHED TO ELLIPTICAL CONE

The surface (21) becomes composite if, e.g., a coaxial elliptical cylinder is attached to the cone base. Let its cross-sectional semi-axes, $\tilde{B}$ and $\tilde{C}$, be parallel to, but neither larger than nor necessarily proportional to B and C (Section III, Fig. 1). With larger-base or rotated cylinders, the description complicates without calling for materially differing concepts.

Since the cone and cylinder axes coincide, the same length variable, σ, and the same angle ρ may be used for both surfaces. But, excepting the case where $\tilde{B} : \tilde{C} = B : C$, the variable τ must be replaced by a variable $\tilde{\tau}$ which will be connected with ρ by the equation

$$\tilde{B} \tan \rho = \tilde{C} \tan \tilde{\tau}$$

analogous to the elliptic relation (23). The points on the cylindrical surface

$$\frac{y^2}{\tilde{B}^2} + \frac{z^2}{\tilde{C}^2} = 1$$

may be represented in the form

$$\left.\begin{aligned} x &= a\sigma \\ y &= \tilde{B} \cos \tilde{\tau} \\ z &= \tilde{C} \sin \tilde{\tau} \end{aligned}\right\}. \tag{32}$$

The same two sets of planes as were used with the cone determine the parametric lines $\tilde{\tau} = \tilde{\tau}^*$ and $\sigma = \sigma^*$ on the cylinder.

The variable σ ranges in the interval

$$\sigma_b \leqq \sigma \leqq \sigma_c$$

if $a\sigma_c$ is the total length of the composite body. That of the cylinder alone will be

$$h = a(\sigma_c - \sigma_b) = x_c - x_b.$$

If again the symmetrical flow vector (25) prevails, it suffices to study the right half of the cylinder. The natural interval in which the variable $\tilde{\tau}$ moves then reduces to

$$-\frac{\pi}{2} \leqq \tilde{\tau} \leqq \frac{\pi}{2} .$$

Both of the intervals will be curtailed by shadow boundaries (except with $\alpha = \pi/2$, when that of σ remains intact). Before establishing the integration limits, the force differential will be set up.

From the general expressions (12), the interior normals are found as

$$n_1 = 0 \qquad n_2 = -\frac{a\,\tilde{C}\cos\tilde{\tau}}{N} \qquad n_3 = -\frac{a\,\tilde{B}\sin\tilde{\tau}}{N}$$

where

$$N = a\left|\sqrt{\tilde{B}^2\sin^2\tilde{\tau} + \tilde{C}^2\cos^2\tilde{\tau}}\right| .$$

On the right half of the cylinder, the component n_2 always points into the negative y-direction ($n_2 < 0$).

It follows that

$$\underline{v} \cdot \underline{n} = -\frac{a\,\tilde{B}\sin\tilde{\tau}\sin\alpha}{N} . \tag{33}$$

As with the cone, the lateral forces cancel ($\tilde{Y} = 0$). The chordwise forces are also zero since the elemental forces are all perpendicular to the x-axis; indeed, $n_1 = 0$. Expression (14) reduces to

$$d^2\tilde{Z} = -4q_\infty a\,\tilde{B}^3\sin^2\alpha\,\frac{\sin^3\tilde{\tau}}{\tilde{B}^2\sin^2\tilde{\tau} + \tilde{C}^2\cos^2\tilde{\tau}}\,d\sigma\,d\tilde{\tau} \tag{34}$$

where the right side has been doubled to compensate for the use planned of only 1/2 the $\tilde{\tau}$-integration interval. The cylinder is affected by the normal forces only.

The tangential shadow line on the cylinder obviously is the generatrix $\tilde{\tau} = 0$ (as can also be seen from the tangential condition $\underline{\nu} \cdot \underline{n} = 0$ which here requires $\tilde{\tau}_t = 0$). The integration interval for $\tilde{\tau}$ therefore is, at most

$$-\frac{\pi}{2} \leqq \tilde{\tau} \leqq 0;$$

it will be even narrower than that when the cast shadow reaches out beyond the cylinder length.

Shielding through the cone's tangential shadow cylinder does not occur as one infers from inspection. The somewhat lengthy analytic proof is omitted here. However, if $\tilde{B} < B$, or $\tilde{C} < C$, the cone's base rim will cause an edge shadow curve to appear on the cylinder's lower surface, cutting off it an unimpinged zone.

The coordinates of points on the elliptic rim line may be written as

$$\left.\begin{aligned} x_r &= x_b \\ y_r &= B \cos \tau \\ z_r &= C \sin \tau \end{aligned}\right\}. \qquad (35)$$

The flow vectors passing through the upper points of the base periphery miss the cylinder, and, except when $\tilde{B} = B$, even the shadow cast by an outer segment of the lower periphery will not strike it. For integration purposes the variable τ thus will move in

$$-\frac{\pi}{2} \leqq \tau \leqq \tau_{max}$$

where the value of τ_{max} is zero or negative. It is associated with the particular generatrix of the shadow cylinder that is tangent to the material cylinder; i.e., that touches it somewhere along the line $\tilde{\tau} = 0$.

The shadow generatrices (19) here have the form

$$y = y_r \qquad \frac{x - x_r}{\cos \alpha} = \frac{z - z_r}{\sin \alpha}.$$

If the cylinder triplets (32) and the rim triplets (35) are introduced, these relations go into

$$\left.\begin{aligned} \tilde{B} \cos \tilde{\tau} &= B \cos \tau \\ (x - x_b) \sin \alpha &= (\tilde{C} \sin \tilde{\tau} - C \sin \tau) \cos \alpha \end{aligned}\right\} \tag{36}$$

where the pairs x_b, τ and x, $\tilde{\tau}$, respectively, identify a point of departure on the (lower) cone base line and the corresponding point of arrival at the cylinder surface.

Since τ_{max} is associated with $\tilde{\tau} = 0$, the first of the relations (36) gives

$$\cos \tau_{max} = \frac{\tilde{B}}{B} \tag{37}$$

which equation, as shown above, must be solved by a negative value (except with $\tilde{B} = B$ where $\tau_{max} = 0$). The x-coordinate, $x_1 = a\sigma_1$, of the point of contact along the line $\tilde{\tau} = 0$ can be obtained from the second equation (36):

$$(x_1 - x_b) \sin \alpha = - C \sin \tau_{max} \cos \alpha.$$

The right side here is not negative, so that $x_1 \geqq x_b$, as one expects.

The cast shadow line on the lower portion of the cylinder thus begins at $\tilde{\tau} = 0$, $\sigma = \sigma_1$ and continues toward the nethermost generatrix, $\tilde{\tau} = - \pi/2$, which value, by the first relation (36), corresponds to $\tau = - \pi/2$. Thus, the abscisa, $x_2 = a\sigma_2$, of the line's low point is given by

$$(x_2 - x_b) \sin \alpha = (C - \tilde{C}) \cos \alpha.$$

The right side again is not negative (since we assume that $\tilde{C} \leqq C$), and therefore $x_2 \geqq x_b$.

If either one of the differences $(x_1 - x_b)$, $(x_2 - x_b)$ is larger than the cylinder length $h = x_c - x_b$, either $\tilde{\tau} = 0$ or $\tilde{\tau} = -\pi/2$ cannot be reached by the cast shadow boundary on the cylinder, and the interval $-\pi/2 \leqq \tilde{\tau} \leqq 0$ must be curtailed accordingly. This can be decided with the aid of the system (36) which in fact is the equation of the shadow curve s_c in terms of the parameter τ. One will have to determine at what value (or values) of $\tilde{\tau}$ the line s_c leaves the cylinder surface. If it does so, the curve s_c (shown in Figure 3) would intersect with the line $\sigma = \sigma_c$, thus extending the cast shadow region and removing a certain domain of negative $\tilde{\tau}$-values from the integration interval.

For simplicity we assume that this is not the case, i.e., that the cylinder is long enough to have an underside area near its rear end fully "illuminated." Regarding the integration over σ, the upper limit will then be the natural limit $\sigma = \sigma_c$. The lower limit, however, will vary according to the variation of σ along the curve s_c whose equation, by eliminating τ from the set (36), can be put into the form

$$\sigma = \sigma_b + \frac{1}{a}\left[\tilde{C}\sin\tilde{\tau} + C\sqrt{1 - (\tilde{B}/B)^2\cos^2\tilde{\tau}}\right]\operatorname{cotg}\alpha = \psi(\tilde{\tau}). \tag{38}$$

The values of σ at the interval terminals, $\tilde{\tau} = 0$ and $\tilde{\tau} = -\pi/2$, are apt to be in any ratio depending on the axis ratios $\tilde{B}/B$ and $\tilde{C}/C$. As one would also expect, there is an extremum at $\tilde{\tau} = -\pi/2$, either a maximum or a minimum. If $(\tilde{B}/B)^2 \geqq (\tilde{C}/C)$, a second extremum (a minimum) may exist. Figure 3 is a schematical sketch of the geometry involved, drawn up in the $(\tilde{\tau},\sigma)$-plane. Half of the natural $\tilde{\tau}$-interval must be excluded on account of the tangential shadow line, s_t, while in the rest area the natural σ-interval is trimmed down by the cast shadow boundary, s_c.

The integration with regard to σ proceeds from $\sigma = \psi(\tilde{\tau})$ to $\sigma = \sigma_c$ (increasing values). The second-order differential (34) then yields the first-order differential

$$d\tilde{Z} = -4q_\infty a \tilde{B}^3 \sin^2\alpha \frac{\sin^3\tilde{\tau}}{\tilde{B}^2\sin^2\tilde{\tau} + \tilde{C}^2\cos^2\tilde{\tau}}\left[\sigma_c - \psi(\tilde{\tau})\right] d\tilde{\tau}.$$

The quadrature in $-\pi/2 < \tilde{\tau} < 0$ will be carried out for two types of cylinders where it is relatively easy.

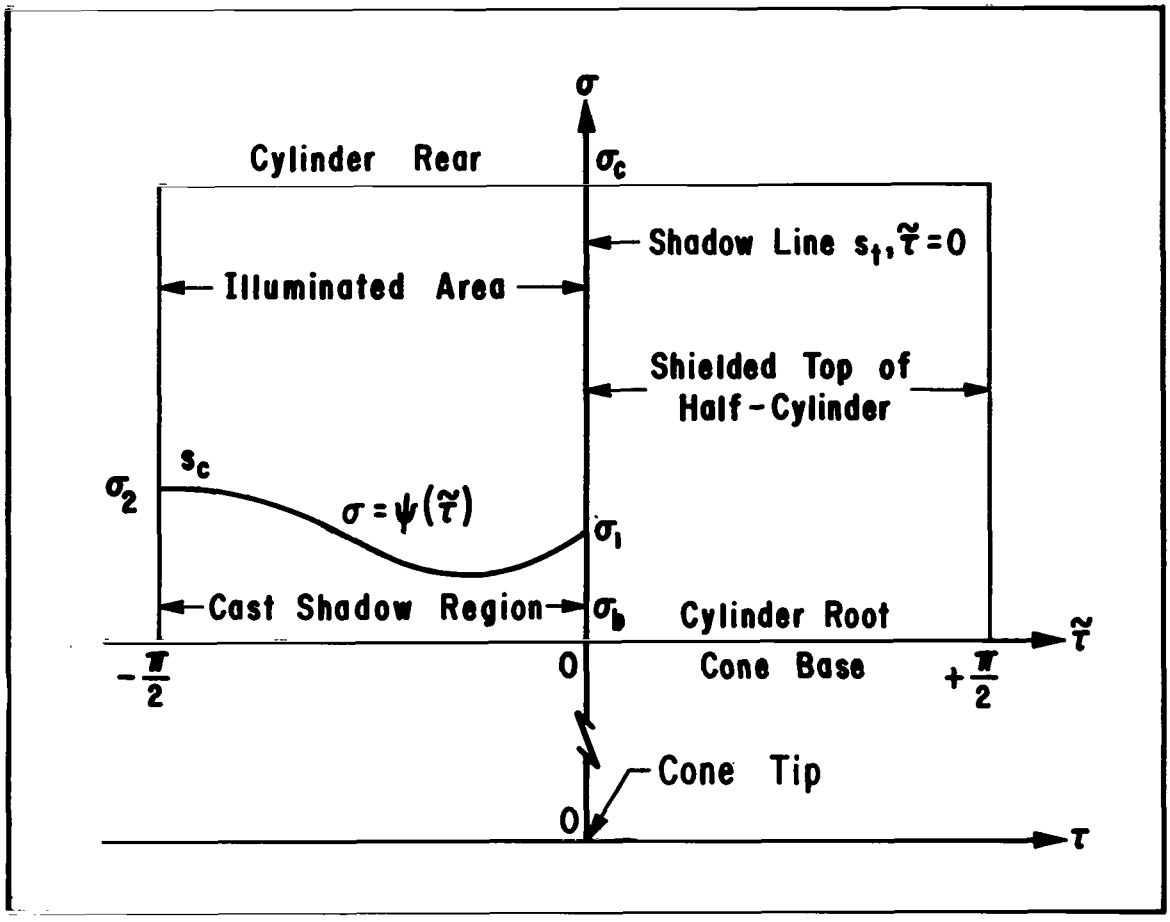

Figure 3. Shadow Geometry on Attached Cylinder (Schematic)

A. The cylinders touch the major axis terminals of the cone base ($\tilde{B} = B$). The curve s_c descends here from the maximum σ_2 to a minimum σ_1 at $\tilde{\tau} = 0$. The functions $\psi(\tilde{\tau})$ and $\tilde{Z}$ take the form

$$\psi(\tilde{\tau}) = \sigma_b + \frac{1}{a}(\tilde{C} - C) \sin \tilde{\tau} \operatorname{cotg} \alpha$$

$$\tilde{Z} = 4q_\infty B \sin^2\alpha \left[\frac{h}{1-\lambda} \left(1 - \frac{1}{2} \frac{\lambda}{\sqrt{1-\lambda}} \ln \frac{1+\sqrt{1-\lambda}}{1-\sqrt{1-\lambda}} \right) \right. \tag{39}$$

$$\left. - \frac{\pi}{4} (C - \tilde{C}) \frac{2\sqrt{\lambda} + 1}{(\sqrt{\lambda} + 1)^2} \operatorname{cotg} \alpha \right]$$

where

$$\lambda = \left(\frac{\tilde{C}}{B}\right)^2 .$$

It is required that

$$h \geq (C - \tilde{C}) \operatorname{cotg} \alpha;$$

the cylinder must have sufficient length to accommodate the entire shadow boundary s_c. Otherwise, $\tilde{Z}$ assumes a different form.

Two special cases stand out here:

(a) $\tilde{C} = C$: the cylinder root is flush with the cone base. The curve s_c reduces to $\sigma = \sigma_b$, meaning that there is no shadow cast on the cylinder. The expression (39) for $\tilde{Z}$ loses the subtractive second term in the brackets (as it would in cross-flow, $\alpha = 90°$).

(b) $\tilde{C} = 0$: the cylinder degenerates into a horizontal plate of width 2B and length $h \geq C \operatorname{cotg} \alpha$. The cast shadow curve (36) is the ellipse

$$\left(\frac{x - x_b}{C \operatorname{cotg} \alpha}\right)^2 + (y/B)^2 = 1.$$

A limiting process required as $\lambda \to 0$ carries expression (39) into

$$\tilde{Z} = Bq_\infty \sin^2\alpha \, (4h - \pi C \operatorname{cotg} \alpha) \geq BCq_\infty \sin 2\alpha \left(2 - \frac{\pi}{2}\right).$$

For comparison, the Z-component for a fully impacted circular cone ($\alpha \leq \omega$, $q = 0$) follows from the second expression in the system (29) as

$$Z = \pi BCq_\infty \sin 2\alpha \cos^2\omega, \quad (B = C),$$

so that the lift of the composite body will be noticeably larger than that of the cone alone. The drag is less affected, although enlarged, too.

B. The cylinders are circular, $\tilde{C} = \tilde{B} = R$, $B \geqq C \geqq R$. The quantity

$$\beta = \frac{\tilde{B}}{B} = \frac{R}{B}$$

is at most equal to unity, so that the square root in $\psi(\tilde{\tau})$ is real. Expression (38) tells that

$$\sigma_1 = \psi(0) = \sigma_b + \frac{C}{a}\sqrt{1 - \beta^2}\ \operatorname{cotg}\alpha$$

$$\sigma_2 = \psi(-\pi/2) = \sigma_b + \frac{C - R}{a}\ \operatorname{cotg}\alpha\ .$$

The curve s_c ascends from the minimum σ_2 to the ordinate σ_1 at $\tilde{\tau} = 0$ (which is not a maximum). The rear end of the cylinder is fully illuminated if

$$\sigma_c \geqq \sigma_1,$$

or if the cylinder length, $h = a(\sigma_c - \sigma_b)$, satisfies the condition

$$h \geqq C\sqrt{1 - \beta^2}\ \operatorname{cotg}\alpha,$$

on which we will base the force computation.

The differential $d\tilde{Z}$ simplifies, since here

$$\tilde{B}^2 \sin^2\tilde{\tau} + \tilde{C}^2 \cos^2\tilde{\tau} = R^2;$$

one obtains from it

$$\tilde{Z} = 4q_\infty R \sin^2\alpha \left\{\frac{2}{3}h + C \operatorname{cotg}\alpha \left[\frac{3\pi}{16}\frac{R}{C} + \left(\frac{1}{8} - \frac{\beta^2}{2}\right)\frac{\operatorname{arc\ sin}\beta}{\beta^3} - \frac{\sqrt{1-\beta^2}}{\beta^2}\left(\frac{1}{8} + \frac{\beta^2}{4}\right)\right]\right\}$$

$$\approx 4q_\infty R \sin^2\alpha \left\{\frac{2}{3}h + C \operatorname{cotg}\alpha \left[\frac{3\pi}{16}\frac{R}{C} - \frac{2}{3} + \frac{\beta^2}{15} + \frac{\beta^4}{160} + O(\beta^6)\right]\right\}.$$

The force decreases with decreasing cylinder radius and cylinder length (which, however, must not sink below the above lower bound; otherwise, $\tilde{Z}$ would be a different expression). If the normal force coefficient is referred to the longitudinal cross section, 2Rh,

$$C_{\tilde{Z}} = \frac{4}{3}$$

with $\alpha = 90°$, which is the known value for a circular cylinder in Newtonian cross flow (Ref. 2, p. 10).

In calculating the moment, $\underline{\tilde{M}}$, of the forces $d^2\tilde{Z}$ one best takes the cone tip (the origin) as the point of reference again. The integration over σ of expression (15) extends from $\sigma = \psi(\tilde{\tau})$ to $\sigma = \sigma_c$. One finds that

$$\underline{\tilde{M}} = 2j\, q_\infty\, a^2 \tilde{B}^3 \sin^2\alpha \int_{-\pi/2}^{0} [\sigma_c^2 - \psi^2(\tilde{\tau})] \frac{\sin^3\tilde{\tau}}{\tilde{B}\sin^2\tilde{\tau} + \tilde{C}\cos^2\tilde{\tau}}\, d\tilde{\tau}.$$

The remaining integrand is elliptic except in the case A ($\tilde{B} = B$) where the square root in the expression for ψ vanishes. Taking this case for illustration,

$$\underline{\tilde{M}} = -2j\, q_\infty \frac{a^2 B}{\tilde{\epsilon}^2} \sin^2\alpha \left\{ (\sigma_c^2 - \sigma_b^2) \left(1 - \frac{1 - \tilde{\epsilon}^2}{2\tilde{\epsilon}} \ln \frac{1 + \tilde{\epsilon}}{1 - \tilde{\epsilon}} \right) + \right.$$

$$\left. + \frac{\pi}{2} \sigma_b \Delta \frac{(2 - 3\tilde{\epsilon}^2) - 2(1 - \tilde{\epsilon}^2)^{3/2}}{\tilde{\epsilon}^2} + \Delta^2 \left[\frac{3 - 5\tilde{\epsilon}^2}{3\tilde{\epsilon}^2} - \frac{(1 - \tilde{\epsilon}^2)^2}{2\tilde{\epsilon}^3} \ln \frac{1 + \tilde{\epsilon}}{1 - \tilde{\epsilon}} \right] \right\},$$

where

$$\Delta = \frac{C - \tilde{C}}{a} \operatorname{cotg} \quad , \qquad \tilde{\epsilon} = \frac{\sqrt{B^2 - \tilde{C}^2}}{B} \, .$$

Since the minor cylinder semi-axis, $\tilde{C}$, is always smaller than the major semi-axis, B, the numerical eccentricity, $\tilde{\epsilon}$, of the cylinder cross-section can never become zero. The largest value that $\tilde{C}$ may attain is $\tilde{C} = C$ when the cylinder and cone bases are congruent ($\tilde{\epsilon} = \epsilon$) and $\underline{M}$ assumes the much shorter form

$$\underline{\tilde{M}} = -2j\, q_\infty \frac{B \sin^2\alpha}{\epsilon^2} (x_c^2 - x_b^2) \left(1 - \frac{1 - \epsilon^2}{2\epsilon} \ln \frac{1 + \epsilon}{1 - \epsilon}\right),$$

which we will use in the following. The condition $\underline{\tilde{M}} = \underline{\tilde{M}}^*$ then gives

$$\tilde{x}^* = \frac{x_c + x_b}{2} . \tag{40}$$

Thus, the centroid of the cylinder is at its midpoint, as one should expect, since a cast shadow does no longer exist.

The cylinder and cone moments both refer to the origin and can be vectorially added to obtain the total moment. The centroid of the total force can then be shown to have the abscissa

$$x^*_{tot} = \frac{x^* Z + \tilde{x}^* \tilde{Z}}{Z + \tilde{Z}} ,$$

when sought out on the body axis. If, again for simplicity, we assume the cone as fully illuminated ($\alpha \leq \omega$), then from expressions (29), (31), (39) and (40)

$$x^*_{tot} = \frac{\frac{2\pi}{3} C x_b \cos\alpha \frac{1 - \sqrt{1 - q}}{\cos^2\omega} + \frac{x_c^2 - x_b^2}{2} \sin\alpha \left(1 - \frac{1 - \epsilon^2}{2\epsilon} \ln \frac{1 + \epsilon}{1 - \epsilon}\right)}{\pi C \cos\alpha (1 - \sqrt{1 - q}) + (x_c - x_b) \sin\alpha \left(1 - \frac{1 - \epsilon^2}{2\epsilon} \ln \frac{1 + \epsilon}{1 - \epsilon}\right)}$$

where the abbreviations

$$q = \epsilon^2 \cos^2\omega \quad \text{and} \quad \lambda = (C/B)^2 = 1 - \epsilon^2$$

have been used. The angle α can become 0°, but not 90°. In the first case $x^*_{tot} = x^*$ (cone centroid), since the cylinder, though flush with the cone, is not impinged at all. With very long cylinders, $x^*_{tot} \to \tilde{x}^*$.

If the cross sections are circular ($\epsilon \to 0$),

$$x^*_{tot} = \frac{2}{3} \frac{\pi C x_b \cos\alpha + (x_c^2 - x_b^2) \sin\alpha}{\pi C \cos\alpha \cos^2\omega + \frac{4}{3}(x_c - x_b) \sin\alpha} .$$

Here, C is the common radius of the cylinder root and cone base.

V. THE BIPARABOLIC CONOID

With an elliptical cone the expressions (28) for the force components ($\alpha > \omega$) are lengthy. More concise formulations can be presumably achieved in the same flow if, in the (x,y)-plane, a sharp edge exists on the surface, preventing the formation of a tangential shadow line. For example, a body may be constructed whose cross sections parallel to the plane x = 0 (Figure 1) are bounded by two symmetric parabolic arcs facing each other and intersecting in the ground plane z = 0. Consider the two parabolas (parameter a > 0)

$$y^2 = 2a(z_o \mp z)$$

in the plane $x = x_o > 0$, with the upper (lower) sign applying in the upper (lower) half-plane. The two finite arcs emerging with the restriction $0 \leq |z| \leq z_o$ enclose the area

$$\frac{8}{3} z_o \sqrt{2a\ z_o},$$

since z = 0, $y = \pm\sqrt{2a\ z_o}$ are their common points, and z_o is their height. Writing now

$$y^2 = 2a\ (x \tan\omega \mp z) \tag{41}$$

we obtain a body whose cross-sectional areas are biparabolic and taper off toward zero if $x \to 0$; there is a tip at the origin. The body roughly resembles the elliptical cone illustrated in Figure 1, with which it will be compared. The plane y = 0 intersects with it in the straight lines

$$x \tan\omega \mp z = 0$$

which have the slope tan ω and, incidentally, are the only straight lines on the surface. The planform (in the plane $z = 0$) is the rim parabola

$$y^2 = 2ax \tan \omega; \tag{42}$$

it is not a triangle as with the cone. The tip angle, ω, the body length, x_b, and the parabola parameter determine the length of the "semi-axes" (Figure 4)

$$\hat{C} = x_b \tan \omega, \quad \hat{B} = \sqrt{2ax_b \tan \omega}$$

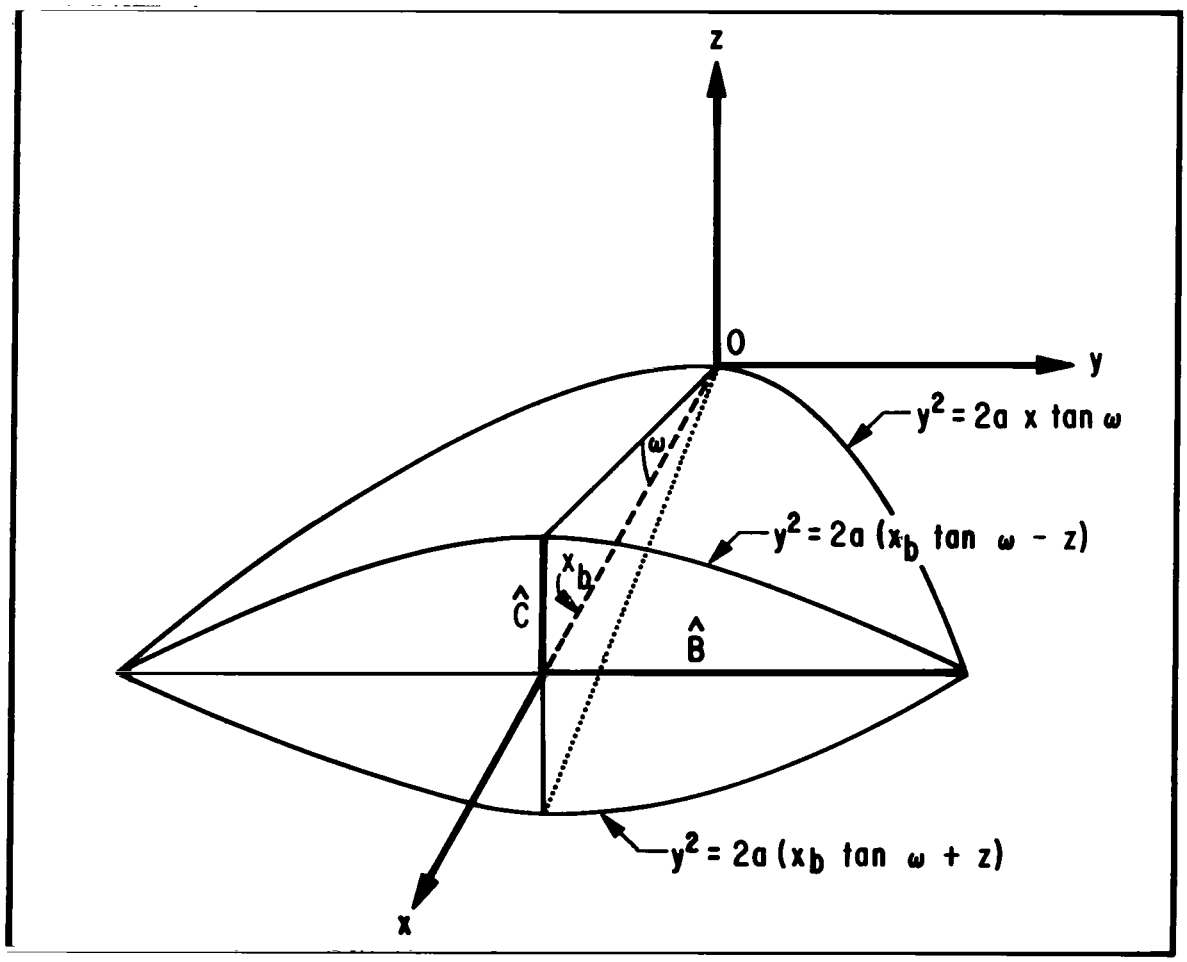

Figure 4. The Biparabolic Conoid

If $\hat{B}$ and $\hat{C}$ remain small while x_b grows large, the body assumes an arrow-like appearance. If, on the other hand, the parabola parameter (a) is very large and ω remains small, a wing-like structure emerges. The volume of the body is

$$\frac{16}{15}\,\hat{B}\,\hat{C}\,x_b,$$

almost equal to that of an elliptical cone $(\frac{\pi}{3}\,BC\,x_b)$ of equal length and equal base axes. The bigger planform is offset by the smaller cross sections (their area ratiosare 4/3 and $8/3\pi$, respectively).

One verifies readily that the surface (41) can be given the pointwise representation

$$\left.\begin{aligned} x &= 2a\sigma^2 \\ y &= 2a\sigma\tau \\ z &= \pm\, 2a\sigma^2(\tan\omega - \tau^2) \end{aligned}\right\}. \tag{43}$$

The natural range of the variable σ is

$$0 \leqq \sigma \leqq \sigma_b, \tag{44a}$$

corresponding to $0 \leqq x \leqq x_b$. Again, from

$$0 \leqq \pm\ z \leqq x \tan\omega,$$

$$\tan\omega \geqq \tau^2 \geqq 0,$$

and thus,

$$-\sqrt{\tan\omega} \leqq \tau \leqq \sqrt{\tan\omega}\,. \tag{44b}$$

The negative values of τ cause y to be negative, while the parenthesis in the expression for z is always positive (or zero).

Both sets of the parametric curves (10) are planar, since the coordinates (43) depend in the second degree only on σ and τ. The curves $\sigma = \sigma^*$ (second family) are the biparabolic arcs. The curves $\tau = \tau^*$ contain the origin (with $\sigma = 0$) and are therefore in the planes

$$z = \pm (\tan \omega - \tau^{*2})x, \quad y = 2a\sigma\tau^* \text{(arbitrary)}$$

through the y-axis. The angle, χ, they make with the (x,y)-plane is given by

$$\tan \chi = \pm (\tan \omega - \tau^{*2}),$$

which relation, since τ^* may be any one value within the range (44b) imparts a geometric meaning to the variable τ.

For finding the shape of the curves $\tau^* = \text{const.}$, consider one of the planes, fixed by, say, a positive value of χ (upper sign). The rotation

$$x = \xi \cos \chi - \zeta \sin \chi$$

$$y = \eta$$

$$z = \xi \sin \chi + \zeta \cos \chi$$

carries this plane into the plane $\zeta = 0$. By the system (43), the curve τ^* in it is described by

$$\xi \cos \chi = 2a\sigma^2$$

$$\eta = 2a\sigma\tau^*;$$

elimination of σ gives

$$\eta^2 = 2a\tau^{*2}\, \xi \cos \chi = 2a(\tan \omega - \tan \chi)\, \xi \cos \chi.$$

The first family therefore consists of parabolas cut out of the conoid by planes through the y-axis. The planform (42) is one of them, corresponding to $\chi = 0$, or to $\tau^{*2} = \tan \omega$. It will be observed that, quite generally, the right parabola branch ($y > 0$) is associated with a positive value of τ^*, the left one with the oppositely equal negative value. Moreover, the same two values appear with two parabolas, one on the upper half ($\chi > 0$) of the body, the other on the lower half ($\chi < 0$). The force components must be set up separately for the two halves (the body is composite, in fact).

The straight ridge lines are characterized by $\chi = \pm \omega$, or $\tau^* = 0$. The parabolas grow more slender if χ approaches $\pm\omega$ and finally degenerate into a straight line. At the same time $|\tau^*|$ becomes smaller and is zero at the end.

From relations (12) the interior normals are found as

$$n_1 = \frac{\sin \omega}{\sqrt{1 + (2\sigma\tau \cos \omega)^2}}, \qquad n_2 = - \frac{2\sigma\tau \cos \omega}{\sqrt{1 + (2\sigma\tau \cos \omega)^2}},$$

$$n_3 = \mp \frac{\cos \omega}{\sqrt{1 + (2\sigma\tau \cos \omega)^2}}$$

while

$$N = \frac{8a^2\sigma^2}{\cos \omega} \sqrt{1 + (2\sigma\tau \cos \omega)^2}.$$

The upper sign refers to the body part in the upper half space.

If the flow vector, as with the cone, is given by expression (25) (the particles arriving from below and behind parallel to the (z,x)-plane), equation (18) assumes the form

$$\sin (\omega \mp \alpha) = 0.$$

There can be no tangential shadow line on the lower part of the body (as is evident from inspection). On the upper part, a shadow line s_c exists with $\alpha = \omega$ only; it coincides with the upper ridge-line, encloses no area and does not affect the forces ($C_p = 0$ along it).

The shadow cylinder through the rim parabola (42) is found to have the rim points only in common with the body so that a cast shadow curve, in the proper sense, does not exist either. However, the rim evidently will act as shadow boundary in certain circumstances. To discuss these, we consider a particle path piercing the ground plane $z = 0$ on or outside the rim parabola. It intersects with the upper surface, i.e., the moving particle will strike it, if

$$\tan \omega \operatorname{cotg} \alpha \geqq 1.$$

The proof, omitted here, starts out with a point on the upper surface and follows the path backward toward its intersection with the ground plane. The choice of the point is completely arbitrary so that we can say: as long as $\alpha \leqq \omega$, the entire upper surface will be impinged upon; with $\alpha > \omega$ none of it will. Instead of the α-dependent shadow line τ_t (cone formula (27)), we have here the fixed boundary

$$\tau = \pm\sqrt{\tan \omega}$$

with $\alpha > \omega$. The force expressions will be simpler accordingly. Application of formula (14) gives

$$d^2\underline{P} = \frac{16q_\infty a^2 \sin^2(\omega \mp \alpha)}{\cos \omega} \frac{\sigma^2}{1 + 4\sigma^2\tau^2 \cos^2\omega} (i \sin \omega - 2j\sigma\tau \cos \omega \mp k \cos \omega) d\sigma d\tau$$

where the upper sign refers to the elemental forces attacking the body's upper half. On integrating over the τ-interval

$$-\sqrt{\tan \omega} \leqq \tau \leqq \sqrt{\tan \omega}$$

the j-component is found to vanish ($dY = 0$) leaving us with

$$d\underline{P} = \frac{16q_\infty a^2 \sin^2(\omega \mp \alpha)}{\cos^2\omega} \sigma \arctan (\sigma\sqrt{2 \sin \omega}) (i \sin \omega \mp k \cos \omega) d\sigma.$$

Further integration over the natural range $0 \leqq \sigma \leqq \sigma_b$ results in

$$X = 2q_\infty a^2 \frac{\sin^2(\omega \mp \alpha)}{\cos^3\omega} [(1 + m^2) \arctan m - m]$$

$$Z = \mp X \operatorname{cotg} \omega$$

where

$$m = \sigma_b \sqrt{2 \sin 2\omega} = \sqrt{\frac{x_b}{a} \sin 2\omega} .$$

With the use of this abbreviation, the conoid's base area, to which the force component will be referred, may be written as

$$\frac{4}{3} a^2 (m/\cos \omega)^3 .$$

Take at first $\alpha > \omega$ (lower signs apply alone). Then, by the system (30),

$$\left.\begin{aligned} C_D &= \frac{3}{2} A \frac{\sin^3(\omega + \alpha)}{\sin \omega} \\ C_L &= \frac{3}{2} A \frac{\sin^2(\omega + \alpha) \cos (\omega + \alpha)}{\sin \omega} \end{aligned}\right\} \alpha > \omega$$

where

$$A = \frac{(1 + m^2) \arctan m - m}{m^3} .$$

These expressions are considerably more compact than the corresponding cone formulas arising with the systems (28) and (30). It is seen that with a sufficiently large angle of attack ($\omega + \alpha > 90°$) the lift coefficient is negative indicating that the aerodynamic force then seeks to drive the body beneath the instantaneous flight direction.

With $\alpha \leqq \omega$, the upper part of the body is impinged upon also, and the force components involving the upper signs must be added to the lower part components:

$$\left.\begin{aligned} C_D &= 3A \cos\alpha \,[\sin^2\omega \cos^2\alpha + 3 \cos^2\omega \sin^2\alpha] \\ C_L &= 3A \sin\alpha \,[\cos^2\omega\,(\cos^2\alpha - \sin^2\alpha) + \cos^2\alpha\,(\cos^2\omega - \sin^2\omega)] \end{aligned}\right\} \alpha \leqq \omega.$$

The lift coefficient here is positive up to at least $\omega = 45°$, with $\alpha \to 0°$ up to $\omega = 54°$. The corresponding figures for the elliptical cones are $\omega = 36°23'$ and $\omega = 41°49'$, respectively.

With $\alpha = \omega$ both sets of expressions give

$$\left.\begin{aligned} C_D &= 12A \sin^2\omega \cos^3\omega \\ C_L &= 3A \cos\omega \sin 2\omega \cos 2\omega \end{aligned}\right\} \alpha = \omega.$$

The force coefficients thus remain continuous if the upper surface passes from full illumination ($\alpha < \omega$) into full darkness ($\alpha > \omega$). Indeed, with $\alpha = \omega$, $X_{upper} = 0$, $Z_{upper} = 0$, meaning that the flow vector, $\underline{v}$, is then tangential to the upper surface everywhere.

One may compare the force coefficients to those of an equivalent cone having the same base area, the same length, and the same tip angle, ω. In these circumstances the cone base major semi-axis, B, is smaller than $\hat{B}$ (Figure 4); $B = \frac{8}{3\pi}\hat{B}$, while $C = \hat{C}$. As a consequence, the volume of the conoid is by 20 percent larger than that of the equivalent cone.

Using the formulas (29) one finds that the cone's lift decreases with its length, x_b; it remains non-negative even with $x_b \to 0$, if

$$\tan^2\alpha \leqq \frac{2 - 3 \sin\omega}{1 - \sin\omega}.$$

(This must be satisfied in addition to $\tan\alpha \leqq \tan\omega$.)

If R_L and R_D denote the lift and drag ratios, respectively, of the conoid and cone, one can, for small angles of attack, derive the expressions

$$R_L \approx \frac{3}{2} AK \frac{(2\cos^2\omega - \sin^2\omega)(1 + K \sin \omega)}{K(2\cos^2\omega - \sin^2\omega) - \sin \omega}$$

$$R_D \approx \frac{3}{2} AK \sin \omega$$

where

$$K = \sqrt{1 + (x_b/B)^2}.$$

Use has been made here of the relations

$$q = \cos^2\omega - (3\pi/16)^2 m^2 = 1 - K^2 \sin^2\omega$$

which follow from the equivalence as stipulated above.

As long as the ratio R_L is positive, it increases with ω, ranging from $R_L \approx 1$ (when $\omega = 0$) to $R_L \approx \infty$ (when the cone lift is zero).

The drag ratio increases from $R_D \approx 0$ (at $\omega = 0$) to $R_D \approx 1$ (at $\omega = \pi/2$). Thus, if $\alpha \approx 0$, the conoid's lift is larger than that of the equivalent cone; its drag is smaller, although the conoid has the larger volume.

Comparisons when α is appreciable, or when $\alpha > \omega$, have not been made; the formulations grow rather unwieldy then.

The location of the centroid on the conoid's axis again does not vary with angle of attack:

$$x^* = \frac{x_b}{2\cos^2\omega}\left\{1 + (1 - 2\sin^2\omega)\frac{m + \frac{2}{3}m^3 - (m^2 + 1) \text{ arc tgm}}{m^2[-m + (m^2 + 1) \text{ arc tgm}]}\right\}.$$

However, there is a dependency on the base shape not found with the elliptical cone. Note that the parameter m may be written as

$$m = \frac{2x_b}{\hat{B}} \sin \omega,$$

while the base area is

$$\frac{8}{3} \hat{B} x_b \tan \omega.$$

If, on varying ω at constant body length, this area is kept constant rather than the semi-axis $\hat{B}$ ($\hat{B} = \bar{B}$ cotg ω, $\bar{B}$ = const., $\hat{C} = x_b \tan \omega$), the body volume

$$\frac{16}{15} \hat{B} x_b^2 \tan \omega$$

will also remain constant, but the general appearance will change from wide and flat (wing-like) at $\omega \approx 0$ to narrow and high (rafter-like) at large values of ω. It can be shown that in these circumstances the centroid abscissa keeps increasing with increasing values of ω, just as it does with the elliptical cone.

With two special tip angles the location of the centroid is independent of the choice of $\hat{B}$.

A limiting process shows that with $\omega = 0$ ($m = 0$)

$$x^* = \frac{3}{5} x_b,$$

which is somewhat smaller than the cone value $x^* = \frac{2}{3} x_b$. The center of gravity is at $x = \frac{5}{7} x_b$. Like the elliptical cone, the conoid is not stable if it is wing-like. One can calculate that stability requires $\omega > 28°$, while with the cones the tip angle must exceed $\approx 20°$. If $\omega = 45°$, $x^* = x_b$. The centroid then coincides with the center of the base. For the elliptical cones this occurs at $\omega \approx 35°$. It appears that the outward movement of the centroid with increasing tip angle is slower with the conoid than it is with the cone.

VI. A BLUNT BODY

The lemniscatic body reported on in Reference 3 was investigated for three reasons: first, to test the general method with a surface of more intricate description, second, to show that the tangential shadow boundary, if not coinciding with a surface coordinate line, may call for close attention as to integration limits and that some of the quadratures required may have to be done numerically, and third, to study a body somewhat similar to the Apollo capsule.

The latter purpose is served better when we now consider a body composed of a right circular cone and a spherical base cap whose radius, R, is rather considerably larger than that of the cone base (B). The mathematical formulations to follow are valid down to R = B, the cap becoming a half-sphere. The angles μ and ρ identified in Figure 5 determine the coordinates of the point P on the sphere:

$$x = R(1 - \cos \mu)$$

$$y = R \sin \mu \cos \rho$$

$$z = R \sin \mu \sin \rho.$$

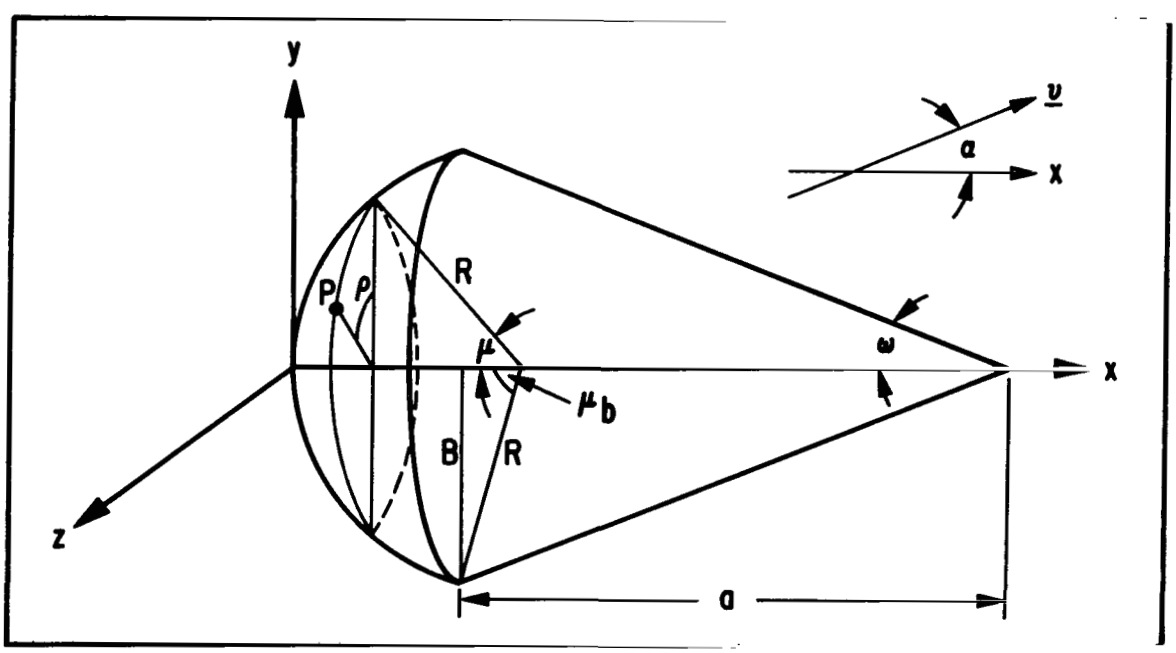

Figure 5. The Blunt Body

They stand for the variables σ and τ in general theory. The parametric curves $\rho = \rho^*$ and $\mu = \mu^*$ are the meridians and the circles of constant latitude on the sphere, respectively. One sees easily that the condition (11), $\Delta = 0$, for planar curves is satisfied. Let $\mu = \mu_b$ denote the latitude of the cone base. The natural intervals then are

$$0 \leqq \mu \leqq \mu_b$$

$$0 \leqq \rho \leqq 2\pi.$$

Expressions (12) give

$$n_1 = \cos \mu, \quad n_2 = - \sin \mu \cdot \cos \rho, \quad n_3 = - \sin \mu \sin \rho$$

$$N = R^2 \sin \mu.$$

If the particles arrive from the lower left,

$$\underline{\nu} = i \cos \alpha + j \sin \alpha,$$

and the condition (18) for the existence of a tangential shadow line on the sphere assumes the form

$$\cos \rho_t = \operatorname{cotg} \alpha \operatorname{cotg} \mu_t.$$

One sees from this that the cap will be fully illuminated if

$$\alpha \leqq \frac{\pi}{2} - \mu_b.$$

Otherwise, the force and moment integrands will contain a term arc cos (cotg α cotg μ), equally unpleasant as the term arc cos (cotg α cotg 3σ) that can never be avoided with the lemniscatic body (Reference 3). It is likely to force a numerical procedure upon us when integrating over μ. Fortunately, the Apollo cap is very flat ($R \gg B$) so that μ_b will be a small angle. Since large angles of attack can be excluded, the tangential shadow line on the cap may be taken as non-existent. The force differential (14) can then be integrated without difficulty, since the fixed

natural limits apply. If the force coefficients are referred to the cone base area, one finds that

$$C_X = \frac{1}{2} \sin^2\alpha \sin^2\mu_b + (1 + \cos^2\mu_b) \cos^2\alpha$$

$$C_Y = \sin \alpha \cos \alpha \sin^2\mu_b$$

$$C_Z = 0.$$

Figure 5 indicates that the unit "a" treated as arbitrary in Sections III and IV is taken here as the cone length. Since $\tau = \rho$ for a circular cone (Figure 2), its point-wise representation may be given as

$$x = a(\sigma_b + 1 - \sigma)$$

$$y = B \sigma \cos \tilde{\rho}$$

$$z = B \sigma \sin \tilde{\rho}.$$

This system follows from the former system (21) by appropriate coordinate transformations. For greater clarity, $\tilde{\rho}$ has been written for ρ, although the meaning of the angle is virtually the same as that of the angle ρ used with the sphere. The variables σ and $\tilde{\rho}$ range in

$$0 \leqq \sigma \leqq 1$$

$$0 \leqq \tilde{\rho} \leqq 2\pi.$$

The values $\sigma = 0$ and $\sigma = 1$ identify the cone tip and the cone base, respectively, so that, when integrating with respect to σ, one moves from tip to base.

From expressions (12), with the use of $B = a \tan \omega$,

$$n_1 = - \sin \omega, \quad n_2 = - \cos \tilde{\rho} \cos \omega, \quad n_3 = - \sin \tilde{\rho} \cos \omega$$

$$N = \frac{B^2\sigma}{\sin \omega}.$$

Condition (18) for tangential incidence becomes

$$\cos \tilde{\rho}_t = - \frac{\tan \omega}{\tan \alpha} .$$

An illuminated area on the cone can exist only if the angle of attack is at least equal to the tip angle ($\alpha \geq \omega$), as one would also infer from inspection. If $\tilde{\rho}_t = \tilde{\rho}^*$ is one solution of this equation, $\rho_t = 2\pi - \rho^*$ will be the other one.

The shadow cylinder through the base periphery can be shown to intersect with the cone in a line wholly confined to the tangential shadow area, so that the integration interval is not curtailed any farther by a cast shadow boundary.

The force differential (14) assumes the form

$$d^2\underline{P} = - 2q_\infty B^2 \sigma \frac{(\sin \omega \cos \alpha + \sin \alpha \cos \omega \cos \tilde{\rho})^2}{\sin \omega} (i \sin \omega + j \cos \omega \cos \tilde{\rho} +$$

$$+ k \cos \omega \sin \tilde{\rho}) \, d\sigma \, d\tilde{\rho}.$$

It needs to be integrated only if $\alpha \geq \omega$ (otherwise, the cone does not contribute to the force). The ranges $0 \leq \sigma \leq 1$ and $\tilde{\rho}^* \leq \tilde{\rho} \leq 2\pi - \tilde{\rho}^*$ must be used. The coefficients, referred to the area πB^2, may be written as

$$\tilde{C}_X = - \frac{\sin^2\alpha \cos^2\omega}{\pi} \left[(1 + 2 \cos^2\tilde{\rho}^*) (\pi - \tilde{\rho}^*) + 3 \sin \tilde{\rho}^* \cos \tilde{\rho}^* \right]$$

$$\tilde{C}_Y = \frac{2 \sin^2\alpha \cos^2\omega}{\pi} \left[(\pi - \rho^*) \cos \tilde{\rho}^* + \frac{\sin \tilde{\rho}^*}{3} (2 + \cos^2\tilde{\rho}^*) \right] \operatorname{cotg} \omega$$

$$\tilde{C}_Z = 0.$$

The brackets here are found to be non-negative in the interval, $< \frac{\pi}{2}, \pi >$, allotted to $\tilde{\rho}^*$; the first varies from $\pi/2$ to zero, the second from 2/3 to zero. Thus, if the cone is struck by the particle stream, it will subtract from the chordwise forces and add to the normal forces of the cap alone.

The centroid of the cap is at $x^* = R$ (even if a tangential shadow line should exist on it), that of the cone is at

$$\tilde{x}^* = x_b + \left(a - \frac{2}{3}\frac{a}{\cos^2\omega}\right),$$

as follows from expression (31) allowing for the changed orientation and denotation (former x_b = present a). Since, from Figure 5,

$$x_b = R(1 - \cos \mu_b)$$

the arm of the total moment will be

$$x^*_{tot} = \frac{RY + \tilde{x}^*\tilde{Y}}{Y + \tilde{Y}} = R + \frac{a - R\cos\sigma_b - \frac{2}{3}\frac{a}{\cos^2\omega}}{Y + \tilde{Y}}\,\tilde{Y}$$

$$= R, \text{ if there are no forces on the cone.}$$

Since

$$\frac{\tilde{Y}}{Y} \leqq \frac{4}{3\pi}\tan\alpha\cos^2\omega\sin^2\mu_b,$$

the centroid of the Apollo configuration, where μ_b is a small angle and $a < R$, will never stray far from the cap's center. On the other hand, the center of gravity will be near the cone base. Since $x_b \ll R$, the configuration should exhibit strong stability in the Newtonian flow regime.

The same can be expected of the Gemini capsule where the rear end of the cone is replaced by a coaxial cylindrical piece. To be sure, if the conical middle part is struck by the particles ($\alpha > \omega$), the deflected stream will come in contact with the cylinder surface, and the Newtonian analysis cannot be applied with confidence. However, the presence of the cylinder should tend to drive the center of pressure still more backward and thus to further stability.

VII. THE MODIFIED APPROACH

With some bodies of plane or axial symmetry and with the circular cylinder in symmetric cross-flow, the Newtonian results have been shown to improve if one sees to it that the pressure coefficient assumes the exact value at the stagnation point where it is usually (because relatively easily computed for $\alpha = 0$). It may be expected that the expression thus gained will also hold good for small angles of attack. At least one corroboration of this surmise exists in the pressure distribution around a circular cone ($\omega = 10°$, $\alpha = 6.7°$) where the modification amounts to a 4 percent increase in values that are already satisfactory on the whole when computed from shockless impact theory.

With the overall angle of attack zero, the angle, ω, at the stagnation point will be the local angle of attack so that $\omega = \frac{\pi}{2} - \alpha'_{stag}$. The modified formula then will be written as

$$C_p = C_p^* \frac{\cos^2\alpha'}{\sin^2\omega} = C_p^* \frac{(\underline{v} \cdot \underline{n})^2}{\sin^2\omega} , \tag{45}$$

where C_p^* is the pressure coefficient at the stagnation point. If $\alpha' = \alpha'_{stag}$, $C_p = C_p^*$ as desired. The value of C_p^* can be calculated from shock transition relations and depends on the ratio of specific heats (γ) in the gas and on the Mach number, M_∞, of the undisturbed flow.

In the case of blunt bodies (for which expression (45) was first suggested in Reference 4) $\sin\omega = 1$ and

$$C_p^* = \frac{2}{\gamma}\frac{1}{M_\infty^2}\left[\left(\frac{\gamma+1}{2}M_\infty^2\right)^{\frac{\gamma}{\gamma-1}}\left(\frac{\gamma+1}{2\gamma M_\infty^2 - \gamma + 1}\right)^{\frac{\gamma}{\gamma-1}} - 1\right]. \tag{46}$$

With infinite Mach number in a diatomic gas, $C_p^* = 1.84$, which figure then replaces the factor 2 of simple impact theory.[p] The values decrease with decreasing Mach number ($C_p^* = 1.64$ for $M_\infty = 2$), at first very slowly; in the hypersonic region $M_\infty \gtrsim 6$ the figure 1.84 may be used throughout with a small error in the second decimal place ($\gamma = 1.4$). Very satisfactory results have been obtained regarding the sphere, ellipsoid- and sphere-capped circular cylinders, and a sphere-blunted circular cone; they were somewhat less accurate with the cylinder in cross-flow. In all cases, however, they surpassed those obtained by another method (Busemann's pressure relief approach).

With plane symmetric bodies having a sharp leading edge to which the shock is attached, one may use the zero incidence stagnation pressure of the wedge which, although it cannot in general be written down explicitly, assumes a convenient form when the cosine of the shock-body angle is sufficiently close to unity. Expression (45) then emerges as

$$C_p = \left[\frac{\gamma + 1}{2} + \sqrt{\left(\frac{\gamma + 1}{2}\right)^2 + \frac{4}{M_\infty^2 \sin^2\omega}}\right] (\underline{v} \cdot \underline{n})^2. \qquad (47)$$

If the Mach number approaches infinity, the bracket approaches $(\gamma + 1)$; the factor 2 is then replaced by 2.4 in a diatomic gas.

With $\gamma = 1.4$, the formula (47) worked well and better than Busemann's method for the wedge itself and for a symmetrical pointed airfoil profile. With the latter and $\gamma = 1.05$, however, the modified Newtonian formula gave consistently too high pressure values and was inferior to the pressure relief approach (which resulted in figures somewhat too small).

The surface of a pointed body of revolution may, near the tip, be approximated by that of a circular cone with the same half opening angle ω. The latter's relation to the angle, σ_s, of the attached shock is involved. As a rule, numerical calculations are necessary, unless both ω and σ_s are small. In this case the approximate expression

$$\frac{C_p^*}{\omega^2} \approx \frac{4}{\gamma + 1}(K_s^2 - 1) + 2(K_s - K)^2 \frac{\gamma + 1}{(\gamma - 1) + \frac{2}{K_s^2}} \qquad (48)$$

is derived in Reference 1 (p. 116-118)*, the relationship of $K = M_\infty \omega$ and $K_s = M_\infty \sigma_s$ being given as

$$\frac{K_s}{K} = \frac{\gamma + 1}{\gamma + 3} + \sqrt{\left(\frac{\gamma + 1}{\gamma + 3}\right)^2 + \frac{2}{\gamma + 3}\frac{1}{K^2}}\,. \qquad (49)$$

*Much of the factual information assembled in the present section is also taken from Chernyi's book.

If $M_\infty \to \infty$,

$$\frac{C_p^*}{\omega^2} \to 2\,\frac{(\gamma + 1)(\gamma + 7)}{(\gamma + 3)^2} = 2.08$$

with $\gamma = 1.4$. The excess over 2 is markedly less than in two dimensions. For the circular cone itself and $\gamma = 1.405$, the approximation of C_p is very good up to $\omega = 20°$, 30°, and 40° if $K \geqq 2, \geqq 3, = \infty$. It breaks rapidly down for $K < 2$, the error amounting to -8 percent at $K = 1$ and $\omega = 5°$. Expression (48) offers an equally satisfactory approximation of the ratio σ_s/ω in terms of K; with ω up to 10°, it is close even with $K = 1$.

A check was also made with an axisymmetric ogive ($\omega = 16.26°$, $M_\infty = 8$, $\gamma = 1.4$). The zero incidence meridional pressure distributions as computed from Newton's modified formula and from the (more exact) numerical method of characteristics were practically identical.

For bodies like the elliptical cone and the biparabolic conoid which are not of rotational symmetry, the modification of the factor 2 must be judged on the basis of the wedge and circular cone results. The flatter these more irregular bodies become at a given value of ω, the more one may be inclined to cautiously upgrade the relative low cone correction. The blunt Apollo-like configuration induces no uncertainty; the modified pressure coefficient will here be smaller in accordance with the general expression (46).

REFERENCES

1. Chernyi, G. G., Introduction to Hypersonic Flow, translated and edited by R. F. Probstein, Academic Press, New York and London, 1961.

2. Truitt, Robert Wesley, Hypersonic Aerodynamics, The Ronald Press Company, New York 1959.

3. Heybey, Willi H., "Newtonian Aerodynamics for General Surfaces," Published in Aero-Astrodynamics Research Review No. 2, NASA TM X-53295, April 1, 1965.

4. Lees, Lester, "Hypersonic Flow," Proc. 5th International Aero. Conf., Los Angeles, Inst. Aero. Sci., New York, 241-276, 1955.

NEWTONIAN AERODYNAMICS FOR GENERAL BODY SHAPES WITH SEVERAL APPLICATIONS

By W. H. Heybey

The information in this report has been reviewed for security classification. Review of any information concerning Department of Defense or Atomic Energy Commission programs has been made by the MSFC Security Classification Officer. This report, in its entirety, has been determined to be unclassified.

This document has also been reviewed and approved for technical accuracy.

E. D. Geissler
Director, Aero-Astrodynamics Laboratory

DISTRIBUTION

INTERNAL

DIR

DEP-T
Dr. Rees

R-ASTR
Dr. Haeussermann
Mr. Kroeger
Mr. Moore
Mr. Hosenthien

MS-IP
CC-P
HME-P
MS-IL (8)
MS-T (6)
R-DIR
Mr. Weidner

R-RP-DIR
Dr. Stuhlinger
Dr. Heller

I-I/IB-DIR
Col. James

R-SA
Mr. Dannenberg
Dr. Kuettner

R-P&VE
Dr. Lucas
Mr. Hellebrand
Mr. Kroll
Mr. Showers
Mr. Blumrich
Mr. Paul
Mr. Palaoro
Mr. Gudzent

R-TEST
Mr. Heimburg
Dr. Reisig

R-AERO
Dr. Geissler
Mr. Jean
Dr. Helmut Krause
Mr. Reed
Mr. Murphree
Dr. Heybey (20)
Mr. Mabry
Dr. Sperling
Mr. McNair
Mr. Thionnet
Mr. Baker
Mr. M. W. Heuser
Mr. Vaughan
Mr. Scoggins
Mr. Dahm
Mr. Holderer
Mr. Linsley (2)
Mr. Wilson
Mr. May
Mr. Clark
Dr. Platzer
Mr. Felix
Mr. Struck
Mr. Sims
Mr. Few
Mr. Andrews
Mr. B. Johnson
Mr. J. Johnson
Mr. Blackwell
Mr. Walker
Mr. Ramsey
Mr. Pitcock
Mr. Morgan
Mr. Young
Mr. McAnally
Mr. Dunn
Mr. Weaver
Mr. Davis
Mr. Donehoo
Mr. Henson
Mr. Nunley
Mr. Lowery
Mr. Bacchus
Mr. Johnston

R-AERO (Cont'd)
Mr. Lindberg
Mr. Garcia
Mr. Stone
Mr. Horn
Mr. Thomae
Mr. Hart

EXTERNAL

Goddard Space Flight Center
Greenbelt, Md.
Attn: John M. Weaver
Library Branch (252)

Donald J. Carlson
Network Engineering Branch (531)
Bldg. 12E, Rm. 124

Ames Research Center
Moffett Field, Calif.
Attn: J. Lloyd Jones, Chief
Vehicle Aerodynamics Br.
Aeronautics Division

William R. Johnson, Chief
Library Branch
Administrative Services Div.

Lewis Research Center
Cleveland, Ohio
Attn: G. Mandel, Head
Library Branch
Technical Information Div.
Administration Bldg., Rm. 208

H. M. Henneberry, Head
Advanced Development and Evaluation Division
8' x 6' SWT Research & Control Bldg., Rm. 112A

NASA Headquarters
Washington, D. C.
Attn: John M. Hetrick, Chief
Headquarters Library, Rm. F60084

Manned Spacecraft Center
Houston, Texas
Attn: O. E. Maynard, Assistant Chief
Apollo Spacecraft Program Office
622 Bldg. 2

Library & Documentation Branch
Technical Information Div.
106 Bldg. 12

W. E. Stoney, Jr., Chief
Advanced Spacecraft Technology Div.
247 Bldg. 16

Langley Research Center
Hampton, Virginia
Attn: J. V. Becker, Chief
Aero-Physics Div.
Research Office
Bldg. 1236

M. R. Nichols, Chief
Full-Scale Research Div.
Bldg. 1212

E. R. Gilman, Chief
Technical Library Section
Research Reports Div.
Bldg. 1244

Northrop Space Laboratories
P. O. Box 4184
Huntsville, Ala.
Attn: E. C. Caldwell, Director
Engineering Technology Section, Dept. 910

Dr. S. S. Hu, Director
Research & Analysis Section, Dept. 920

Douglas Linder, Dept. 910
Gordon Gibbs, Dept. 910
Jack Headley, Dept. 910
Walter Watson, Dept. 910

David R. Carlson
Engineering Technology Section, Dept. 910

EXTERNAL DISTRIBUTION (Continued)

Douglas Aerophysics Laboratory, A-10
2332 El Segundo Blvd.
El Segundo, California
Attn: W. E. Smith, Deputy Chief

Jet Propulsion Laboratory
California Institute of Technology
Pasadena, California
Attn: Bain Dayman, Jr., Assistant Chief
Aerodynamic Facilities Section

JPL Library (2)

Arnold Engineering Development Center
Tullahoma, Tennessee
Attn: James Myers, Engineering, ARO
von Karman Facility

Space and Information Systems Division
North American Aviation, Inc.
Downey, Calif.
Attn: Dr. Ta Li, Principal Scientist
Dynamic Sciences

Charles B. Blumer, Research Scientist
Space Sciences Laboratory

S&ID Library (2)

Ed Allen, Dept. 696-710

Glenn Boyd
Chrysler Corporation Space Division
Dept. 2761
P. O. Box 26018
New Orleans, La.

Technical & Scientific Information Facility (25)
P. O. Box 33
College Park, Md.
Attn: NASA Representative (S-AK/RKT)

Research Institute
University of Alabama
Attn: Dr. Rudolf Hermann
Mr. Thoenes